

Electronic Supplementary Information

Crowding Out: Ligand modification and their structure directing effects on brucite-like $\{M_x(\mu_3\text{-OH})_y\}$ ($M = \text{Co(II)}, \text{Ni(II)}$) core growth within polymetallic cages

*Mari E. Slater-Parry,^a James P. Durrant,^a Joshua M. Howells,^a Mateusz B. Pitak,^c Peter N. Horton,^c Wim T. Klooster,^c Simon J. Coles,^c Helen M. O'Connor,^b Euan K. Brechin,^b Anne-Laure Barra^d and Leigh F. Jones^{*a}*

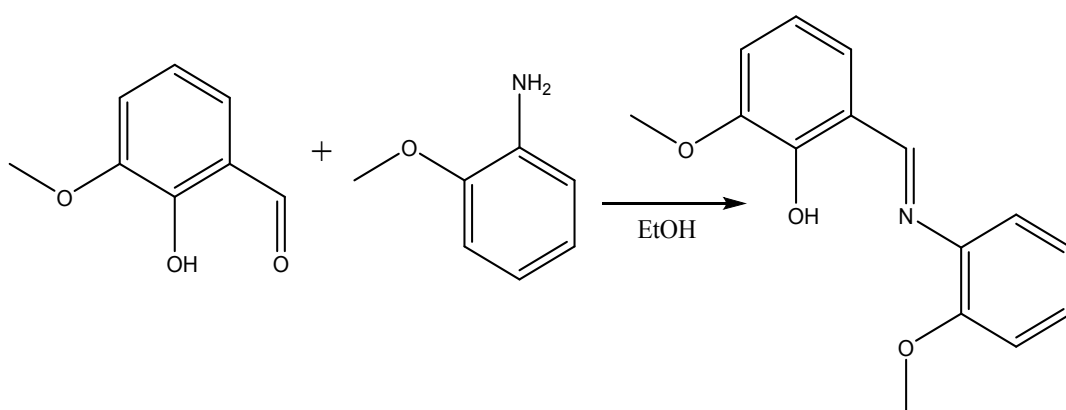
^a School of Natural Sciences, Bangor University, Bangor, Wales, LL57 2DG, UK. Tel: +44(0)1248-38-2391. Email: leigh.jones@bangor.ac.uk

^b EaStCHEM School of Chemistry, David Brewster Road, University of Edinburgh, Edinburgh, Scotland, EH9 3FJ, UK.

^c UK National Crystallographic Service, Chemistry, Faculty of Natural and Environmental Sciences, University of Southampton, England, UK. SO17 1BJ.

^d LNCMI-CNRS, Universite Grenoble-Alpes, Avenue des Martyrs, Grenoble, France.

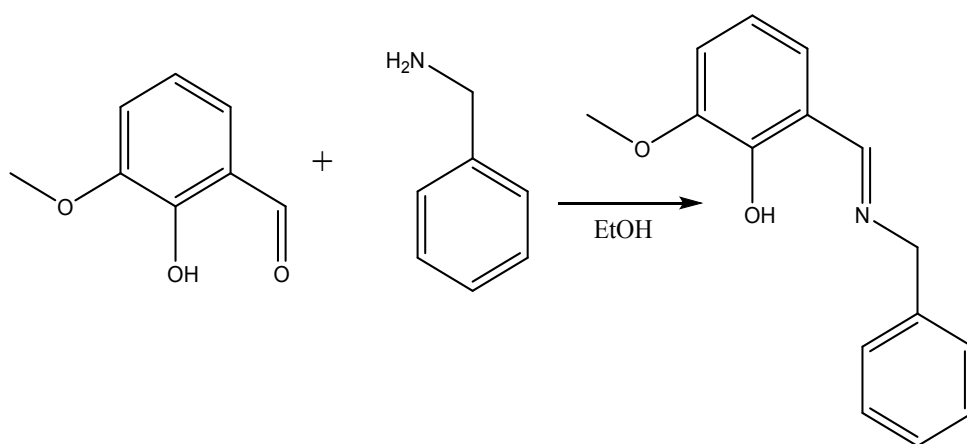
Synthesis of 2-methoxy-6-{[(2-methoxyphenyl)imino)methyl]phenol (L_3H)



Scheme S1: Reaction scheme for the synthesis of 2-methoxy-6-{[(2-methoxyphenyl)imino)methyl]phenol (L_3H).

To a 50 cm³ ethanolic solution was added o-vanillin (3.0 g, 19.72 mmol, 1 eq.) and o-anisidine (2.23 ml, 19.72 mmol). The resultant mixture was allowed to stir at room temperature overnight. The mixture changed from a dark orange to a dark red colour during this time. A precipitate was produced and subsequently filtered off using suction filtration and washed with minimum amounts of solvent (ethanol). The solid was then dried under reduced pressure to give L₃H in 87% yield (4.41 g). ¹H NMR (400 MHz, CDCl₃) δ 8.71 (s, 1H), 7.26 – 7.22 (m, 2H), 6.99 (td, *J* = 9.2, 1.2 Hz, 4H), 6.85 (t, *J* = 7.9 Hz, 1H), 3.94 (s, 3H), 3.90 (s, 3H). ¹³C NMR (100 MHz, CDCl₃) δ 161.48, 153.21, 152.81, 148.91, 136.47, 128.15, 123.62, 121.05, 119.29, 118.10, 114.47, 112.11, 56.26, 55.99. Elemental analysis (%) calculated (found) for L₃H (C₁₅H₁₅N₁O₃): C 70.02 (70.21), H 5.88 (6.02), N 5.44 (5.37). FT-IR (cm⁻¹): 2967 (w), 2836 (w), 1611 (s), 1585 (w), 1574 (w), 1495 (w), 1477 (w), 1455 (s), 1402 (w), 1361 (w), 1335 (w), 1301 (w), 1285 (w), 1273 (m), 1248 (s), 1194 (m), 1172 (m), 1162 (m), 1092 (w), 1078 (w), 1048 (w), 1021 (s), 970 (s), 937 (w), 888 (w), 854 (s), 835 (w), 780 (s), 761 (s), 737 (s), 636 (w), 587 (w), 521 (w), 480 (w). ESI-MS [M⁺] (*m/z*): 257.14.

Synthesis of 2-[(benzylimino)methyl]-6-methoxyphenol (L₄H)

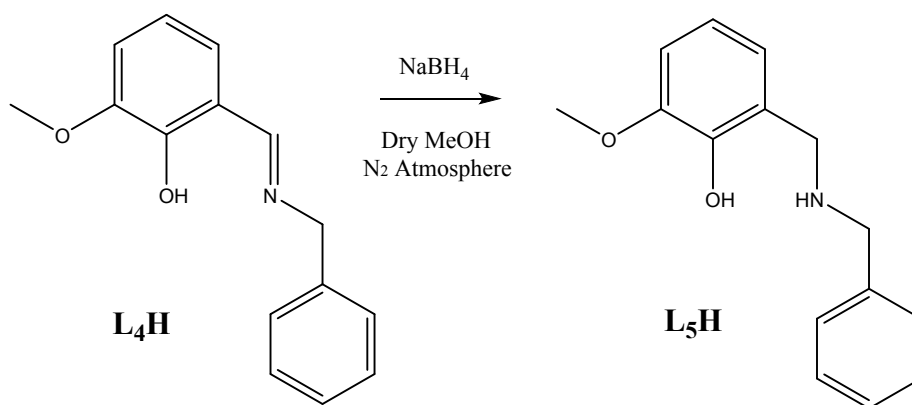


Scheme S2: Reaction scheme for the synthesis of 2-[(benzylimino)methyl]-6-methoxyphenol (L₄H).

To a 100 cm³ ethanolic solution of o-vanillin (4.00 g, 26.3 mmol) was added 2.85 cm³ (26.3 mmol) of benzylamine. The solution was covered in parafilm and left to stir overnight. The resulting solution was concentrated under reduced pressure and then placed into an ice bucket to promote crystallisation. The resultant yellow polycrystalline powder was then dried on a Buchner funnel to afford 6.18 g (98%) of L₄H. ¹H NMR (400 MHz, CDCl₃) δ 13.90 (s, 1H), 8.43 (s, 1H), 7.37 – 7.27 (m, 5H), 6.92 (dd, *J* = 12.8, 7.3 Hz, 2H), 6.82 (t, *J* = 7.8 Hz, 1H), 4.83

(s, 2H), 3.90 (s, 3H). ^{13}C NMR (100 MHz, CDCl_3) δ 165.78, 151.94, 148.63, 138.17, 128.80, 127.76, 127.48, 123.14, 118.76, 118.11, 114.23, 62.84, 56.24. Elemental analysis (%) calculated (found) for L_4H ($\text{C}_{15}\text{H}_{15}\text{N}_1\text{O}_2$): C 74.67 (74.88), H 6.27 (6.41), N 5.81 (5.76). FT-IR (cm^{-1}): 3027 (w), 2997 (w), 2957 (w), 2938 (w), 2884 (w), 2834 (w), 2587 (w), 1630 (m), 1578 (w), 1494 (w), 1459 (s), 1452 (s), 1435 (m), 1413 (m), 1379 (w), 1343 (w), 1332 (w), 1302 (w), 1249 (s), 1187 (w), 1169 (w), 1153 (m), 1081 (m), 1052 (m), 1029 (w), 992 (w), 973 (w), 949 (w), 880 (w), 835 (w), 778 (w), 749 (s), 734 (s), 697 (s), 635 (w), 573 (w), 562 (w), 538 (w), 471 (w), 447 (w). ESI-MS [M^+] (m/z): 241.06.

Synthesis of 2-[(benzylamino)methyl]-6-methoxyphenol (L_5H)



Scheme S3: Reaction scheme for the reduction of ligand L_4H to 2-[(benzylamino)methyl]-6-methoxyphenol (L_5H).

To a 50 cm^3 methanolic solution of L_4H (2.50 g, 10.4 mmol) was added 0.47 g (12.4 mmol) of NaBH_4 . The resultant solution was stirred at room temperature for 18 hours and the solvent subsequently removed under reduced pressure. The clear, yellow tinted oily residue was added to 100 cm^3 of ethyl acetate and 30 cm^3 of saturated potassium carbonate. The aqueous phase was extracted with three 30 cm^3 portions of ethyl acetate and the combined organic extracts were dried (MgSO_4) and concentrated under reduced pressure to afford 2.25 g (89%) of L_5H as a white / light cream solid (Fig. S2). ^1H NMR (400 MHz, CDCl_3) δ 7.33 (s, 5H), 6.83 (d, $J = 8.1$ Hz, 1H), 6.76 (t, $J = 7.8$ Hz, 1H), 6.65 (d, $J = 7.5$ Hz, 1H), 4.03 (s, 2H), 3.89 (s, 3H), 3.84 (s, 2H). ^{13}C NMR (100 MHz, CDCl_3) δ 148.22, 147.33, 138.09, 128.83, 128.64, 127.80,

122.46, 120.91, 118.99, 111.20, 56.07, 52.61, 51.35. Elemental analysis (%) calculated (found) for L₅H (C₁₅H₁₇N₁O₂): C 74.05 (73.28), H 7.04 (7.07), N 5.76 (5.64). FT-IR (cm⁻¹): 3304 (w), 2835 (w), 1584 (w), 1489 (m), 1474 (m), 1453 (m), 1407 (m), 1356 (w), 1262 (w), 1231 (s), 1186 (w), 1094 (w), 1084 (w), 1070 (s), 1055 (w), 1026 (w), 990 (m), 939 (m), 923 (w), 901 (w), 878 (w), 857 (w), 831 (m), 781 (w), 764 (m), 745 (s), 730 (s), 710 (m), 699 (s), 616 (w), 588 (w), 565 (w), 557 (w), 482 (w). ESI-MS [M⁺] (*m/z*): 243.10.

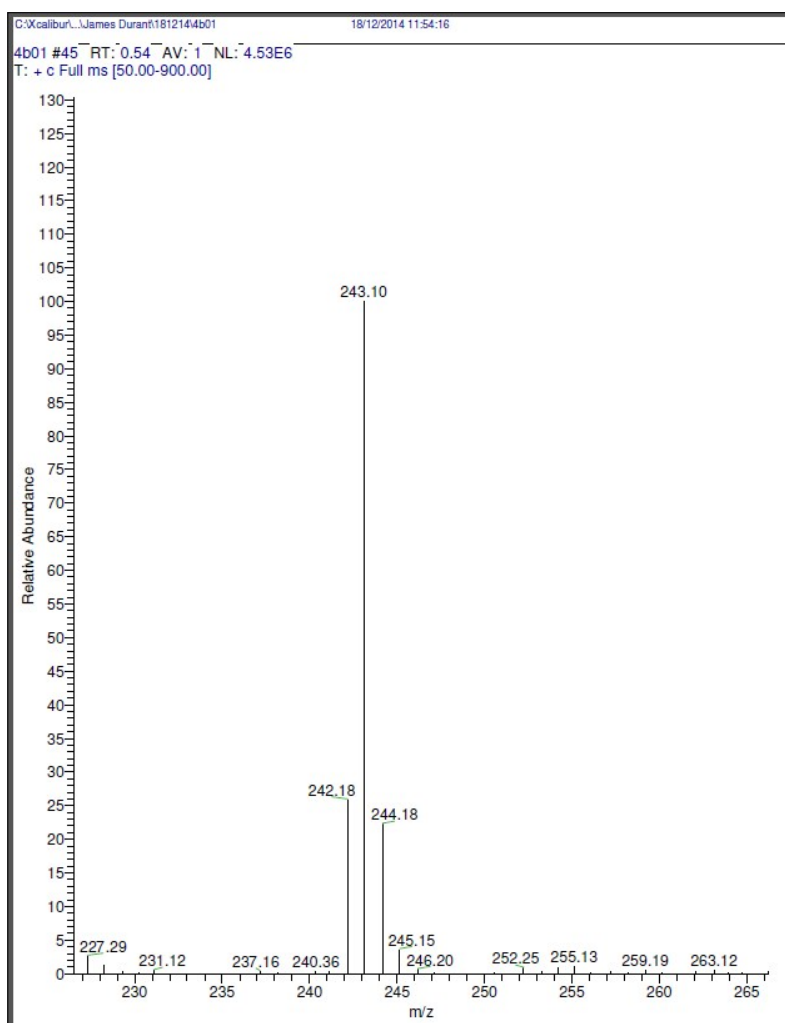


Figure S1 ESI+ Mass spectrum obtained from L₅H.

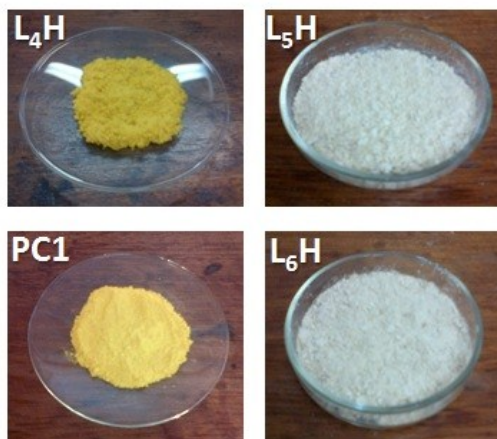
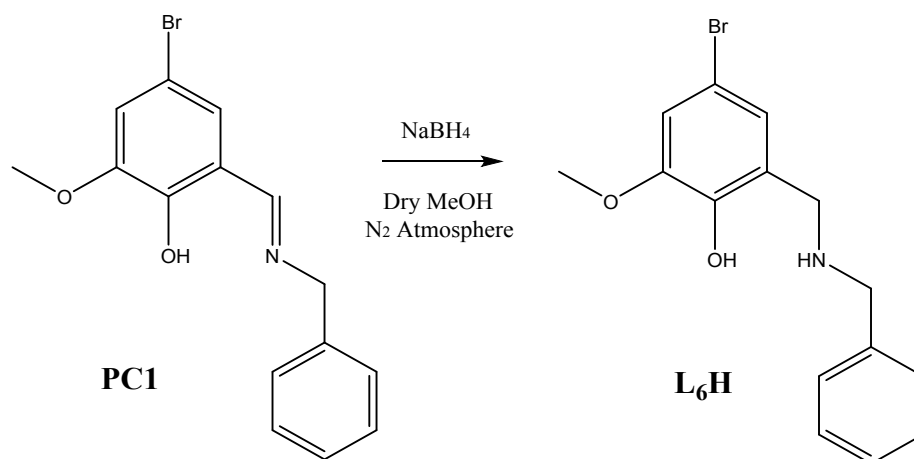


Fig. S2 Samples of ligands **L₄H**, **L₅H**, **L₆H** and **PC1** (precursor to **L₆H**).

Synthesis of 2-[(benzylamino)methyl]-4-bromo-6-methoxyphenol (**L₆H**)



Scheme S4: Reaction scheme for the reduction of ligand **PC1** to 2-[(benzylamino)methyl]-4-bromo-6-methoxyphenol (**L₆H**).

Synthesis of precursor 1 (**PC1**): (E)-2-[(benzylimino)methyl]-4-bromo-6-methoxyphenol (**PC1**)

To a 100 cm³ ethanolic solution of bromo-vanillin (4.00 g, 17.3 mmol) was added 1.90 cm³ (17.3 mmol) of benzylamine. The solution was covered in parafilm and left to stir overnight. The resulting solution was concentrated under reduced pressure and placed into an ice bucket to promote crystallisation. The resultant yellow polycrystalline solid was then dried on a Buchner funnel to afford 5.38 g (97%) of **PC1**. ¹H NMR (400 MHz, CDCl₃) δ 8.26 (s, 1H), 7.35 – 7.28 (m, 2H), 7.23 (d, *J* = 11.8 Hz, 2H), 6.95 (dd, *J* = 12.9, 2.0 Hz, 2H), 4.78 (s, 2H),

3.84 (s, 3H). ^{13}C NMR (100 MHz, CDCl_3) δ 164.54, 151.77, 149.67, 137.57, 128.89, 127.84, 127.69, 125.01, 119.30, 117.14, 109.28, 62.52, 56.42. Elemental analysis (%) calculated (found) for $\text{C}_{15}\text{H}_{14}\text{N}_1\text{O}_2\text{Br}_1$: C 56.27 (56.10), H 4.41 (4.40), N 4.38 (4.21). FT-IR (cm^{-1}): 3436 (vb), 3386 (w), 3014 (w), 2960 (w), 2925 (w), 2834 (w), 1627 (s), 1574 (w), 1489 (s), 1450 (m), 1441 (m), 1376 (m), 1346 (m), 1319 (w), 1256 (m), 1252 (s), 1536 (w), 1081 (w), 1052 (w), 1025 (w), 1001 (w), 981 (w), 843 (m), 820 (w), 757 (m), 734 (w), 710 (m), 702 (w), 660 (w), 607 (w), 574 (m), 492 (w), 453 (w), 416 (w). ESI-MS [M^+] (m/z): 320.98.

Synthesis of 2-((benzylamino)methyl)-4-bromo-6-methoxyphenol (L_6H)

To a methanolic solution (50 cm^3) of PC1 (2.86 g, 8.94 mmol) was added 0.405 g (10.7 mmol) of NaBH_4 . The resultant solution was stirred at room temperature for 18 hours and the solvent was removed under reduced pressure. The clear, yellow tinted oily residue was added to 100 cm^3 of ethyl acetate and 30 cm^3 of saturated potassium carbonate. The aqueous phase was extracted with three 30 cm^3 portions of ethyl acetate and the combined organic extracts were dried (MgSO_4) and concentrated to afford 2.72 g (94%) of L_6H as a white solid (Fig. S4). ^1H NMR (400 MHz, CDCl_3) δ 7.33 (dd, $J = 16.3, 6.1$ Hz, 5H), 6.93 (d, $J = 2.0$ Hz, 1H), 6.77 (d, $J = 2.0$ Hz, 1H), 3.97 (s, 2H), 3.87 (s, 3H), 3.81 (s, 2H). ^{13}C NMR (100 MHz, CDCl_3) δ 148.96, 146.74, 138.11, 128.81, 128.63, 128.47, 127.76, 127.15, 123.95, 123.14, 114.32, 110.37, 56.20, 52.65, 51.21. FT-IR (cm^{-1}): 3454 (vb), 3306 (m), 3292 (m), 3030 (w), 2996 (w), 2933 (w), 2851 (w), 1575 (w), 1483 (s), 1442 (s), 1398 (s), 1358 (m), 1264 (m), 1232 (s), 1212 (m), 1186 (w), 1077 (m), 1025 (w), 991 (m), 951 (w), 911 (w), 858 (m), 829 (m), 752 (s). ESI-MS [M^+] (m/z): 322.41.

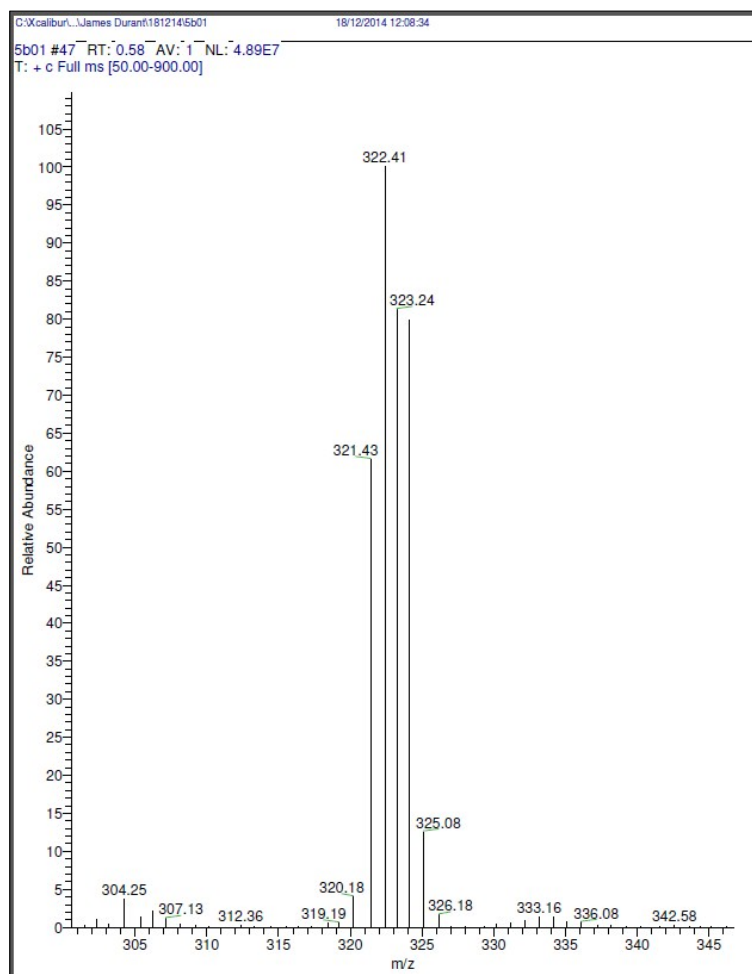


Fig. S3 ESI+ Mass spectrum obtained from L_6H .

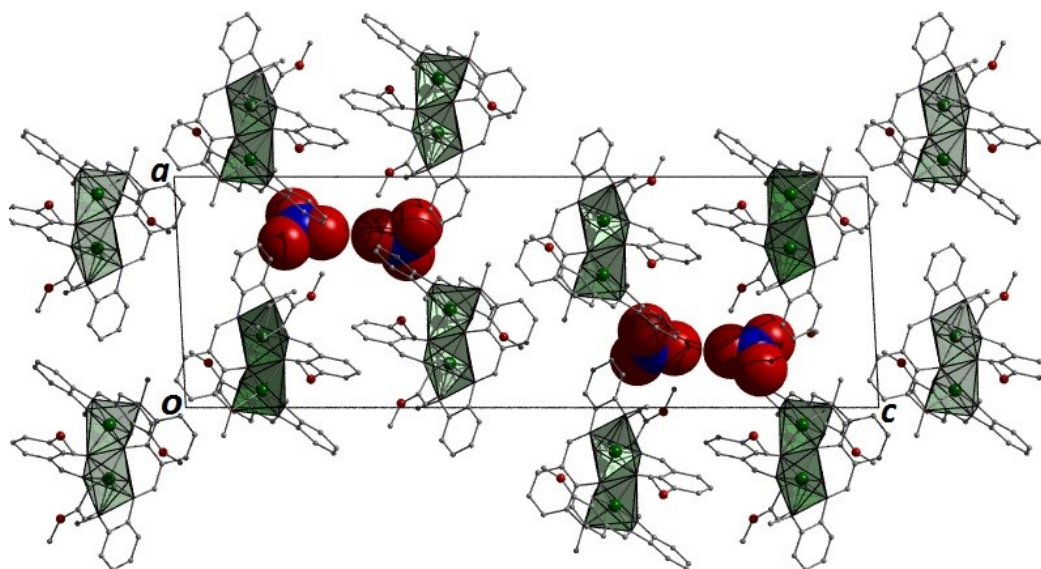


Figure S4 Polyhedral representation of the packing arrangement of $[\text{Ni}(\text{II})_2(\text{L}_4)_3(\text{H}_2\text{O})](\text{NO}_3) \cdot 3\text{MeOH} \cdot \text{H}_2\text{O}$ (**3**) as viewed along the *b* unit cell direction. All solvents of crystallisation have been omitted for clarity. The NO_3^- counter anions are space-fill represented. All hydrogen atoms have been omitted for clarity.

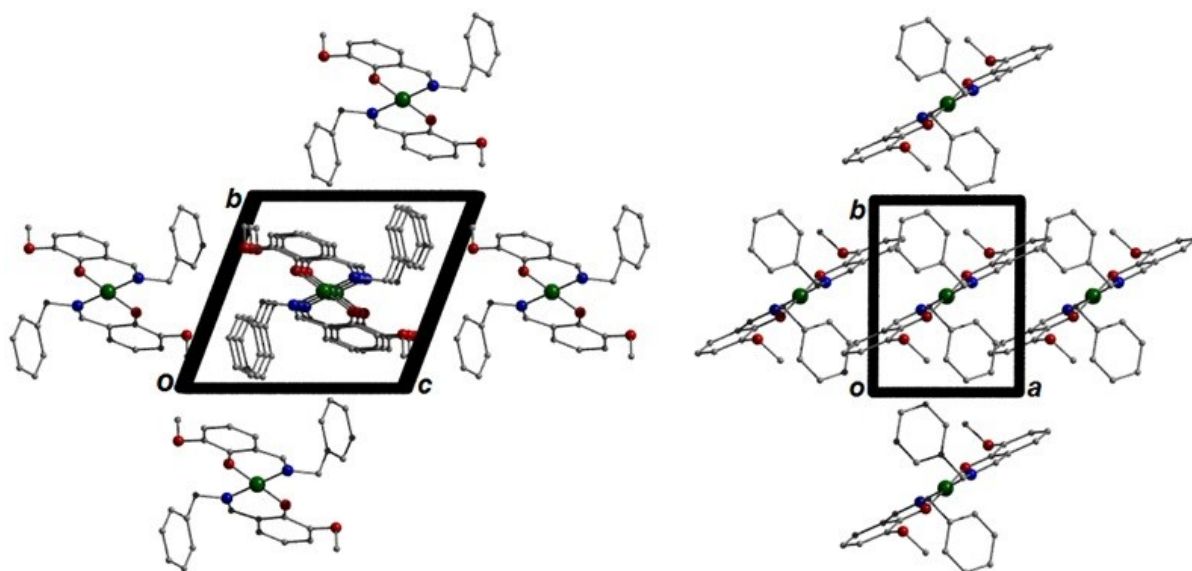


Figure S5 Packing in **4** as viewed down the *a* (left) and *c* (right) cell directions. Hydrogen atoms have been removed for clarity.

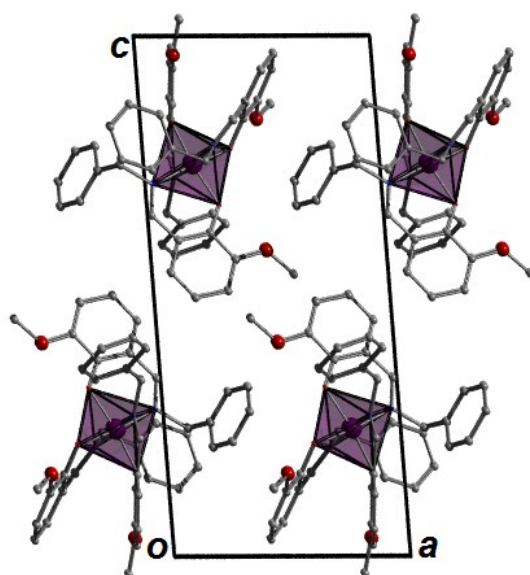


Figure S6 Packing arrangement of $[\text{Co}(\text{III})(\text{L}_4)_3] \cdot \text{MeOH} \cdot \text{H}_2\text{O}$ (**5a**) as viewed along the *b* cell direction. Solvent molecules and hydrogen atoms have been omitted for clarity.

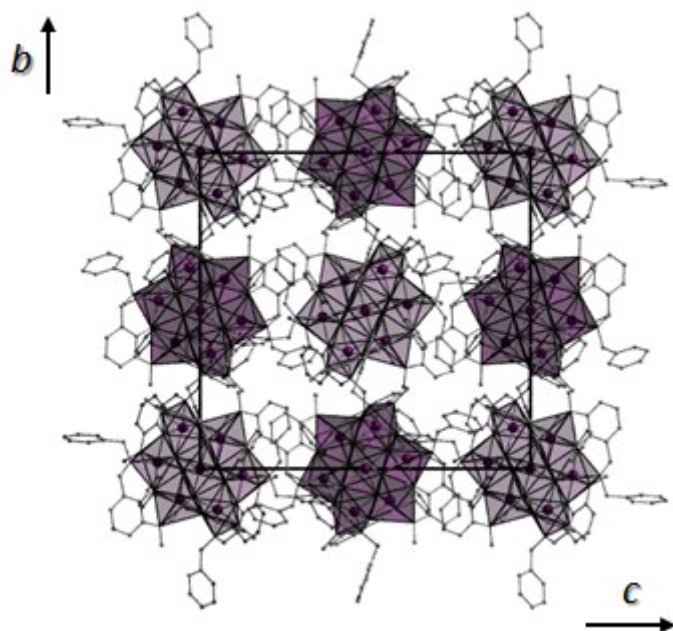


Figure S7 Packing arrangement of the [Co(II)₇] pseudo metallocalix[6]arenes in **5b** as viewed along the *a* direction of the unit cell. NO₃⁻ counter anions and H-atoms have been omitted for clarity.

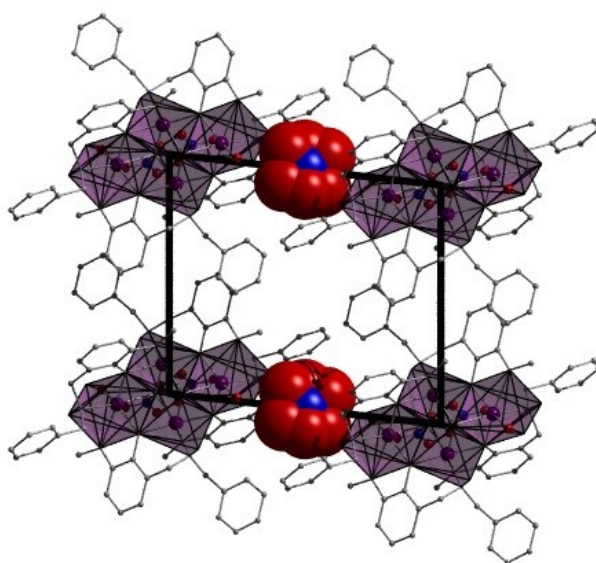


Figure S8 Polyhedral representation of the packing arrangement observed in **6** as viewed along the *a*-axis of the unit cell. Hydrogen atoms have been omitted for clarity and NO₃⁻ anions are space-fill represented.

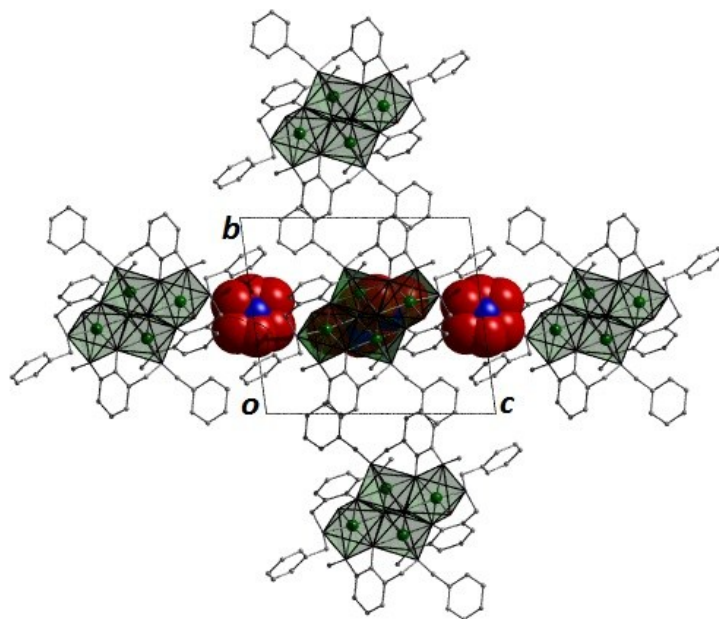


Figure S9 Polyhedral representation of the packing arrangement observed in **7** as viewed along the *a* axis of the unit cell. Hydrogen atoms have been omitted for clarity and NO₃⁻ anions are space-fill represented.

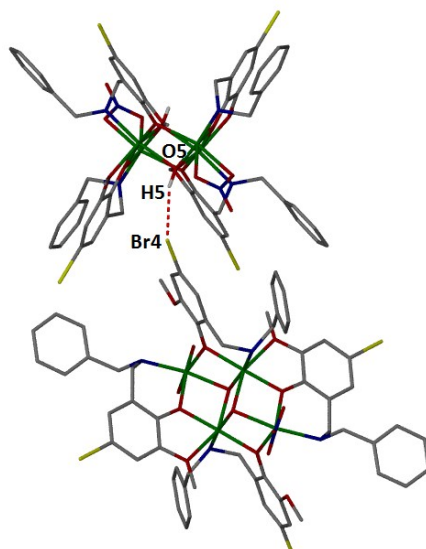


Figure S10 H-bonding interaction (red dashed line) between two {Ni₄} units in **8** (O5(H5)···Br4 = 2.528 Å). Hydrogen atoms omitted for clarity.

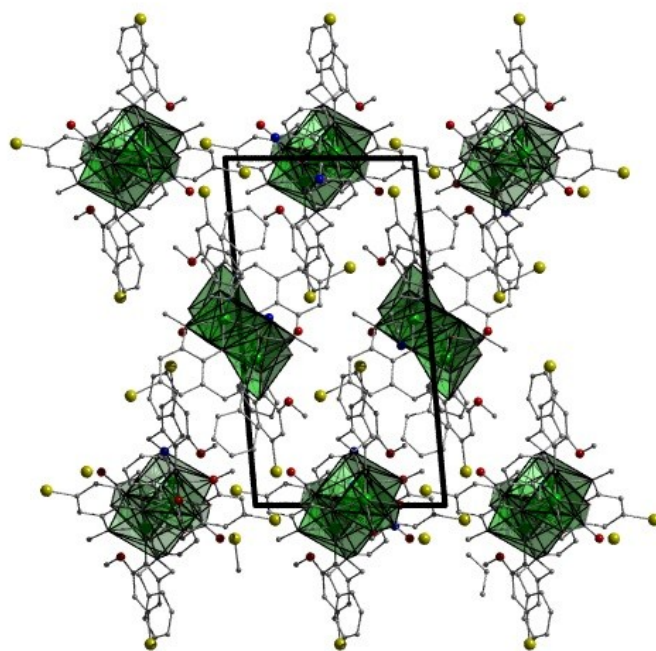


Figure S11 Polyhedral representation of the packing arrangement observed in **8** as viewed along the *b* axis of the unit cell. Hydrogen atoms and NO_3^- anions have been omitted for clarity.

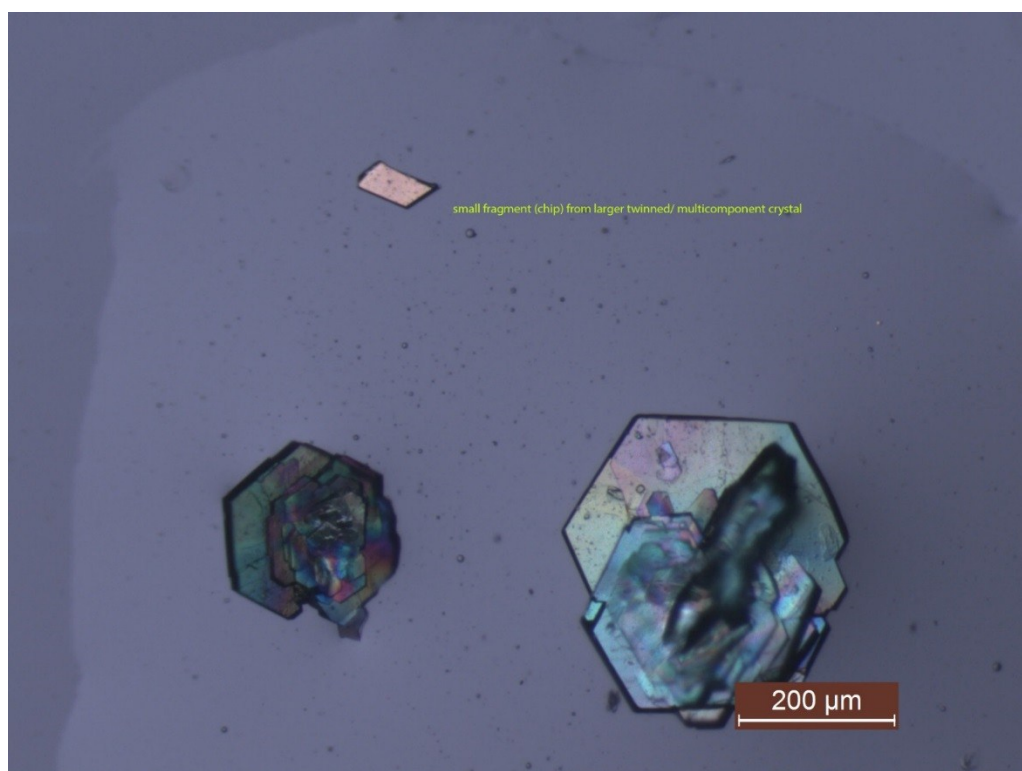


Figure S12 The crystal morphology in **8** showing the small fragment of crystal collected (top middle) after being chipped from a larger twinned multicomponent crystal.

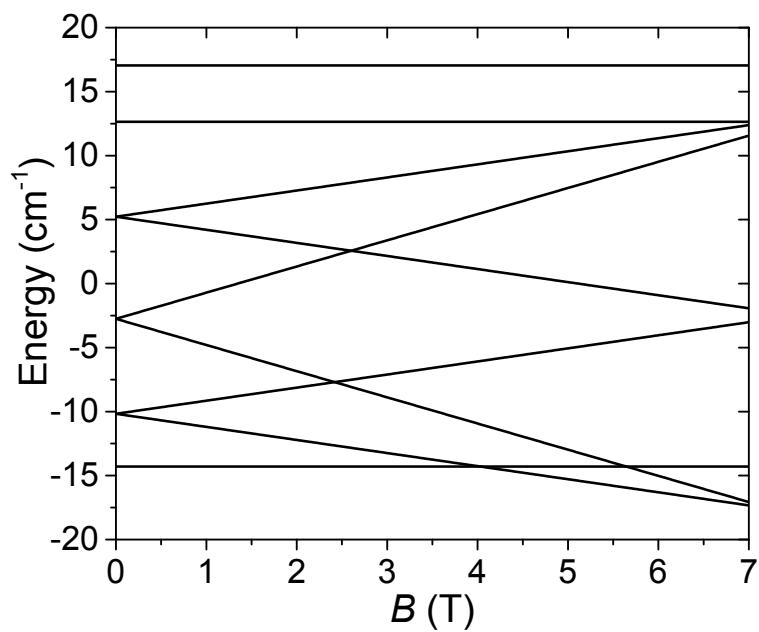


Figure S13 Zeeman diagram for complex (**3**) generated from the best fit parameters obtained from a simultaneous fit of the susceptibility and magnetization data. See main text for details.

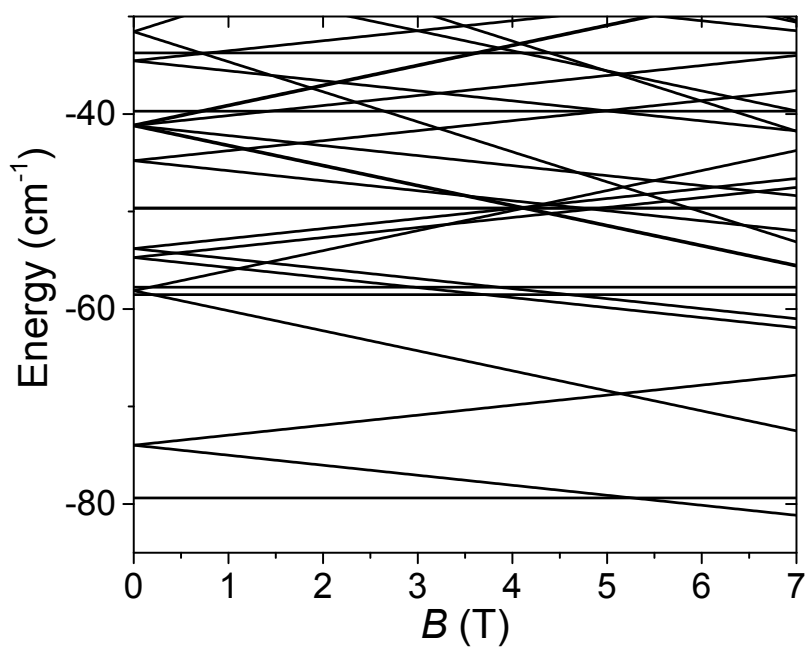
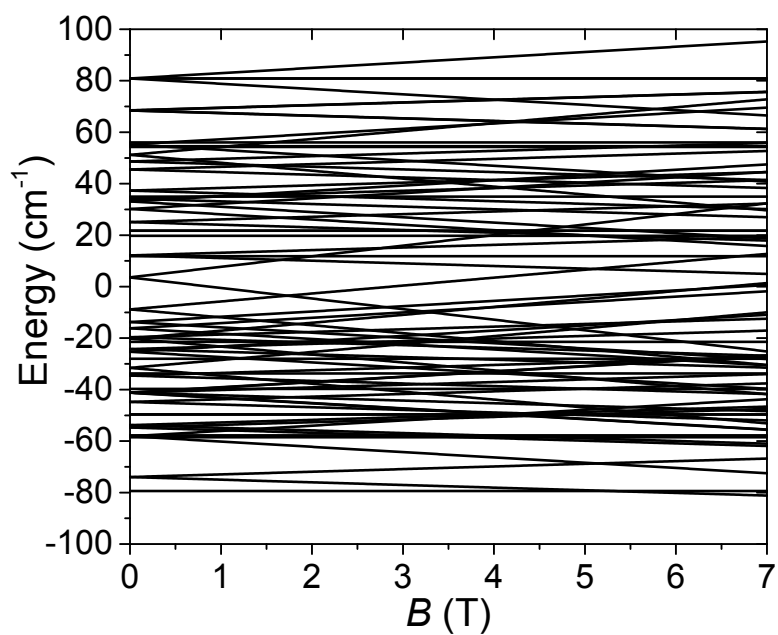


Figure S14 (top) Zeeman diagram for complex (**8**) generated from the best fit parameters obtained from a simultaneous fit of the susceptibility and magnetization data. See main text for details.

(bottom) Zeeman diagram highlighting the lowest lying energy levels for complex (**8**) generated from the best fit parameters obtained from a simultaneous fit of the susceptibility and magnetization data.

See main text for details.

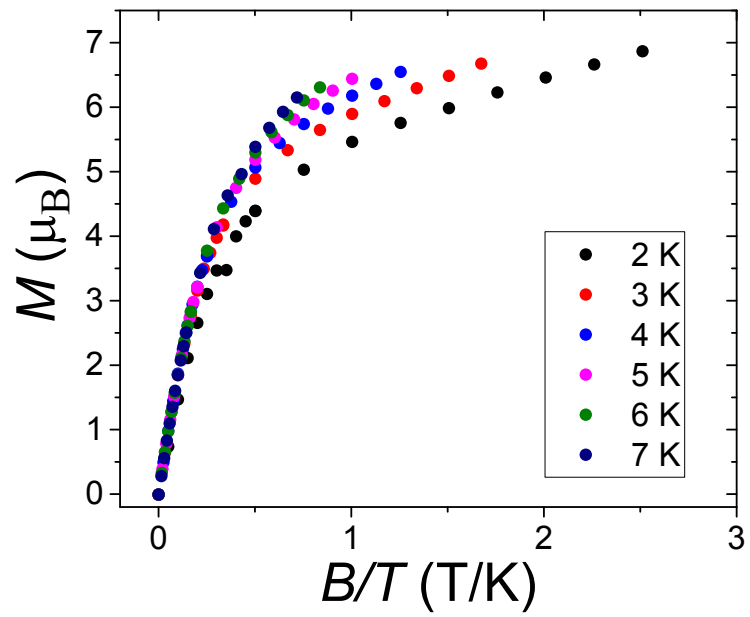


Figure S15 Reduced magnetisation (M/μ_B) vs. B/T (T/K) data obtained from a polycrystalline sample of **6** measured within the 2-7 K temperature range and 0-7 T magnetic field range.

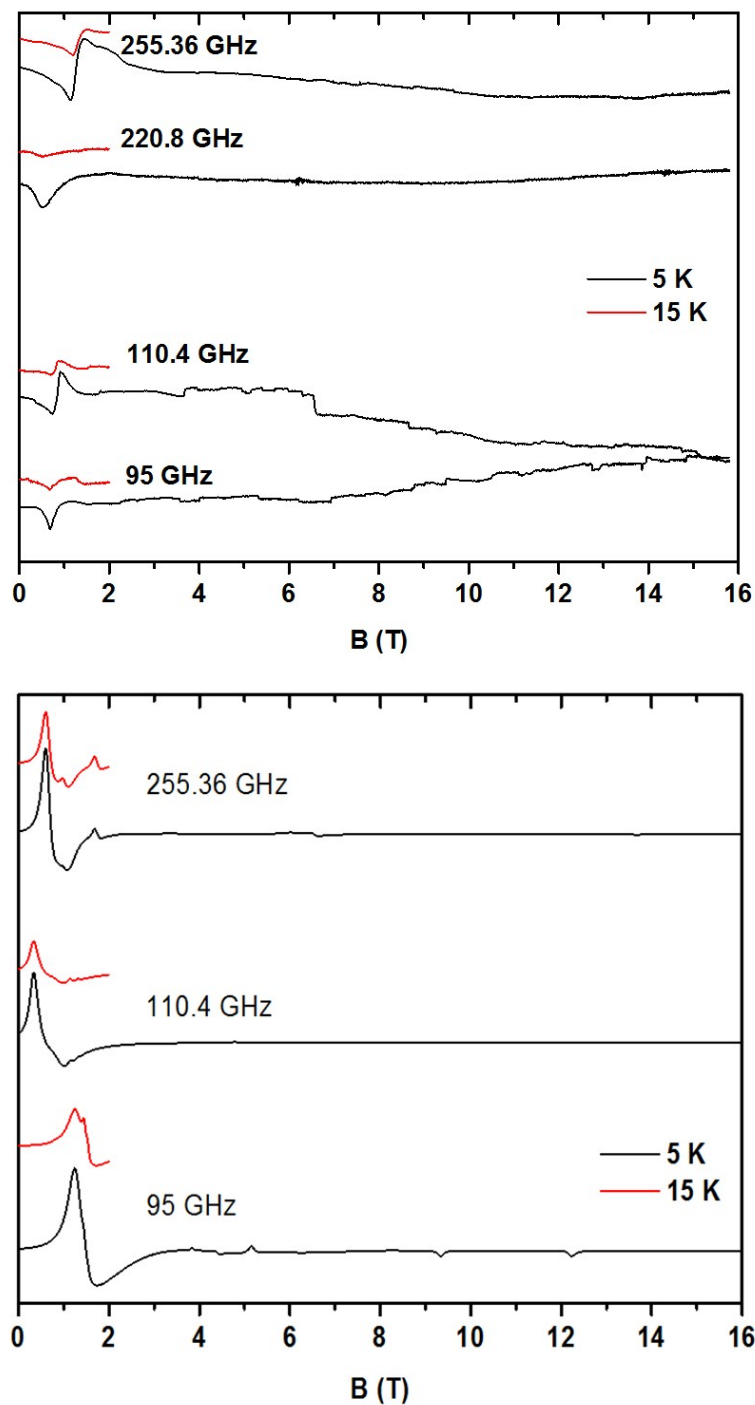


Figure S16 (top) Experimental MF/HF-EPR spectra obtained on a polycrystalline pelletised sample of **3** exhibiting a close to zero field transition. The intensity decrease with the increase of temperature indicates that these signals arise from the ground state spin level. Intensities have been rescaled from one frequency to the other. (Bottom) Simulated MF/HF-EPR spectra of **3** with the multispin model and the parameters described in the main text. Intensities have been rescaled from one frequency to the other.

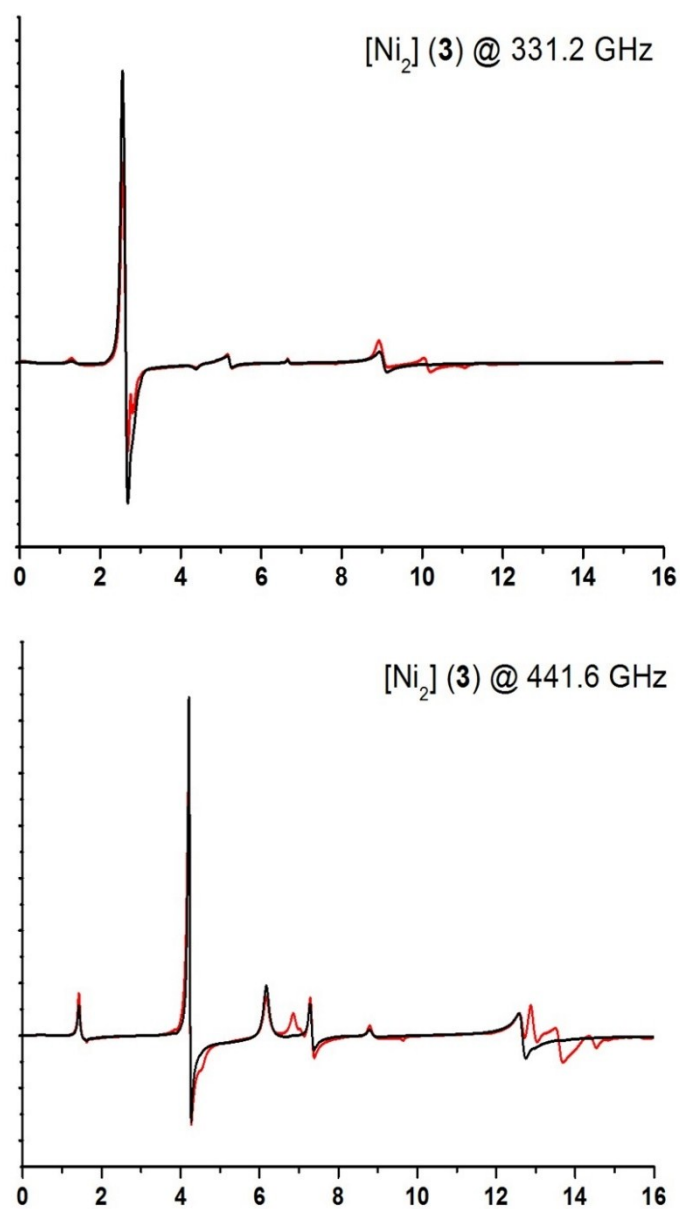


Figure S17 Simulated HF EPR spectra for [Ni₂] (3) at frequencies 331.2 (top) and 441.6 GHz (bottom) at 15 K (red line) and 5 K (black line), using the multispin model and the parameters described in the main text.

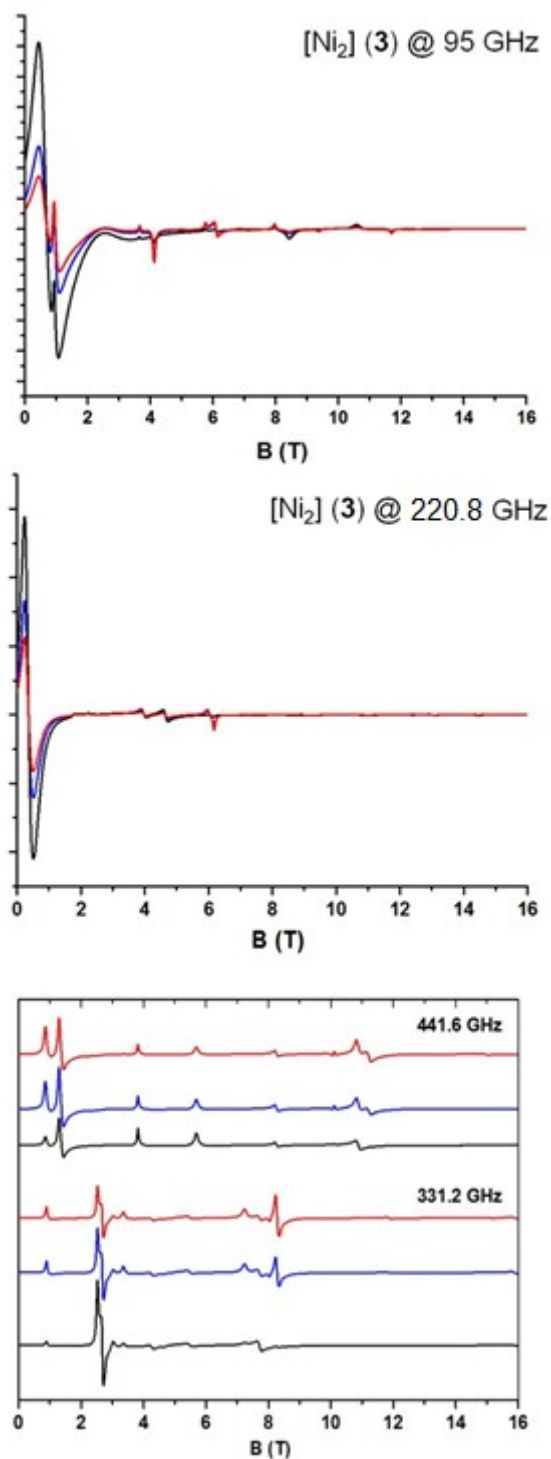


Figure S18 Calculated HF-EPR spectra using a simple $S = 2$ system (Giant Spin model) for $[\text{Ni}_2]$ (**3**) at frequencies 95.0 (top), 220.8 (middle), 331.2 and 441.6 GHz (bottom) at 25 K (red line), 15 K (blue line) and 5 K (black line), with the following parameters: $D_{S=2} = 5.0 \text{ cm}^{-1}$, $E_{S=2} = 0.67 \text{ cm}^{-1}$ and an isotropic $g = 2.2$. These parameters are chosen to reproduce the low field signals (see main text) observed in **3** (for 95-110 GHz and 220-255 GHz frequency ranges). However, conversely to these low field signals and to the forbidden transitions, note that the $S = 2$ calculated allowed transitions at 331.2

and 441.6 GHz fall roughly 2 T lower in field than the experimentally measured resonances (~8 T instead of ~10 T at 331.2 GHz, and ~11 T instead of ~13 T at 441.6 GHz). This strongly indicates the breakdown of the giant spin model, as forbidden transitions are less sensitive to the parameters than allowed transitions. Furthermore, at 441.6 GHz, the two strong simulated signals appearing at approximately ~1 T (when we consider an $S = 2$ descriptor) are not observed experimentally. This is striking because these calculated signals are more intense than the calculated forbidden signal below 4 T (which is clearly observed experimentally).

Table S1 X-ray crystallographic data obtained from complexes **3-5**.

	3 .2H ₂ O.3MeOH	4	5a .H ₂ O.MeOH	5b .0.5H ₂ O.4MeOH
Formula ^a	C ₄₈ H ₆₀ N ₄ O ₁₈ Ni ₂	C ₃₀ H ₂₈ N ₂ O ₄ Ni ₁	C ₄₆ H ₄₈ N ₃ O ₈ Co ₁	C ₉₇ H ₁₁₀ N ₈ O _{28.5} Co ₇
M_w	1098.39	539.25	829.82	2256.48
Crystal System	Monoclinic	Triclinic	Triclinic	Monoclinic
Space group	P2 ₁ /n	P-1	P-1	P2 ₁ /c
$a/\text{Å}$	12.6966(4)	6.7178(3)	10.3690(2)	19.8705(5)
$b/\text{Å}$	10.1709(3)	9.3940(4)	10.7727(3)	22.1327(4)
$c/\text{Å}$	38.0873(11)	10.1699(4)	20.5457(7)	23.1956(4)
$\alpha/^\circ$	90	69.232(4)	85.474(2)	90
$\beta/^\circ$	92.904(3)	87.650(4)	84.339(2)	94.902(2)
$\gamma/^\circ$	90	89.471(4)	63.261(3)	90
$V/\text{Å}^3$	4912.1(3)	599.58(5)	2038.05(10)	10163.8(4)
Z	4	1	2	4
T/K	100(2)	100(2)	100(2)	100(2)
$\lambda^b/\text{Å}$	0.71073	0.71073	0.71073	0.71073
$D_c/\text{g cm}^{-3}$	1.307	1.493	1.271	1.309
$\mu(\text{Mo-K}\alpha)/\text{mm}^{-1}$	0.829	0.851	0.472	1.177
Meas./indep.(R_{int}) refl.	50784 / 8992 (0.0628)	6995 / 3018 (0.0221)	41114 / 7469 (0.0366)	23280 / 19834(0.0726)
Restraints, Parameters	7, 563	0, 170	0, 499	6, 1133
wR2 (all data)	0.1965	0.0889	0.0929	0.3316
$R1^{d,e}$	0.0683	0.0293	0.0469	0.1737
Goodness of fit on F^2	1.057	1.185	1.201	1.335

^a Includes guest molecules. ^b Mo-K α radiation, graphite monochromator. ^c $wR2 = [\sum w(|F_o|^2 - |F_c|^2)|^2] / \sum w|F_o|^2|]^2$. ^d For observed data. ^e $R1 = \sum ||F_o| - |F_c|| / \sum |F_o|$.

Table S2 X-ray crystallographic data obtained from complexes **6-8**.

	6.H₂O	7.H₂O	8.MeCN
Formula ^a	C ₆₀ H ₇₂ N ₆ O ₁₉ Co ₄	C ₆₀ H ₇₂ N ₆ O ₁₉ Ni ₄	C ₆₂ H ₆₅ Br ₄ N ₇ O ₁₆ Ni ₄
<i>M_w</i>	1414.94	1416.07	1718.69
Crystal System	Triclinic	Triclinic	Triclinic
Space group	P-1	P-1	P-1
<i>a</i> /Å	9.0455(6)	9.0156(2)	11.1808(5)
<i>b</i> /Å	12.6133(9)	12.5137(2)	15.8405(5)
<i>c</i> /Å	14.4430(10)	14.5497(2)	20.5877(5)
<i>α</i> /°	92.607(6)	93.1290(10)	105.986(2)
<i>β</i> /°	104.914(6)	105.662(2)	90.324(3)
<i>γ</i> /°	103.757(6)	105.280(2)	105.805(3)
<i>V</i> /Å ³	1536.64(18)	1510.62(5)	3359.9(2)
<i>Z</i>	1	1	2
<i>T</i> /K	100(2)	100(2)	100(2)
<i>λ</i> ^b /Å	0.71073	0.71073	0.71073
<i>D_c</i> /g cm ⁻³	1.529	1.557	1.699
<i>μ</i> (Mo-Kα)/ mm ⁻¹	1.139	2.027	3.553
Meas./indep.(<i>R</i> _{int}) refl.	16789 / 5605 (0.0592)	28299 / 5493 (0.0403)	35525 / 12305 (0.0522)
Restraints, Parameters	8, 440	6, 392	36, 851
wR2 (all data)	0.0968	0.1036	0.1773
<i>R</i> 1 ^{d,e}	0.0454	0.0374	0.0581
Goodness of fit on <i>F</i> ²	1.048	1.028	1.044

^a Includes guest molecules. ^b Mo-Kα radiation, graphite monochromator. ^c $wR2 = [\sum w(|F_o|^2 - |F_c|^2)^2 / \sum w|F_o|^2]^2$. ^d For observed data. ^e $R1 = \sum |F_o| - |F_c| / \sum |F_o|$.

Table S3: BVS calculations on complexes **5a**, **5b** and **6**.

Complex	Atom label and BVS result
(5a)	Co1
	3.22
5b*	Co1 (central)
	1.96
	Co2 (outer ring)
	2.01
	Co3 (outer ring)
	2.03
	Co4 (outer ring)
	2.00
Co5 (central)	
1.96	
	Co6 (outer ring)
	2.05
	Co7 (outer ring)
	1.99
	Co8 (outer ring)
	2.06
6	Co1 (wing-tip)
	1.94

	Co2 (body)
	2.01

* There are two independent $\{\text{Co(II)}_7\}$ units in the asymmetric unit in **5b**.

Mass Spectrometry on complexes **6** and **8** (courtesy of the EPSRC National MS Centre at Swansea University)

The MALDI-TOF mass spectrum of **6** (in DBTC / MeCN matrix) shows many CID fragments with prominent peaks at $m/z = 664$ and 755 representing the $\{[\text{Co(II)}_4(\mu_3\text{-OH})_2(\text{L}_5)_4(\text{H}_2\text{O})_5]\}^{2+}$ and $\{[\text{Co(II)}_4(\mu_3\text{-OH})_2(\text{L}_5)_4(\text{H}_2\text{O})_6(\text{MeCN})_4]\}^{2+}$, respectively. The peaks at $m/z = 1027$ and 1055 are indicative of the fragmentation of the L_5^- ligands (* = loss of pendant C_6H_5^- groups) and represent the $\{[\text{Co(II)}_4(\mu_3\text{-OH})_2(\text{L}_5^*)_4(\text{H}_2\text{O})_2](\text{NO}_3)^+\}$, and $\{[\text{Co(II)}_4(\mu_3\text{-OH})_2(\text{L}_5^*)_4](\text{NO}_3)_2 + \text{H}^+\}$ species, respectively. Complex **8** shows similar fragmentation patterns with peaks at (m/z): 795 , 820 and 873 representing the $\{\text{Ni}_4(\mu_3\text{-OH})_2(\text{L}_6)_4(\text{H}_2\text{O})_2\}^{2+}$, $\{\text{Ni}_4(\mu_3\text{-OH})_2(\text{L}_6)_4(\text{MeCN})_2\}^{2+}$ and $[\text{Ni}_4(\mu_3\text{-OH})_2(\text{L}_6)_4(\text{MeCN})_4(\text{H}_2\text{O})]^{2+}$ species, respectively.